

Article

Mathematical Modeling and Experimental Validation of Surface Roughness in Ball Burnishing Process

Rahul O. Vaishya ¹, Vivek Sharma ¹, Vinod Mishra ², Anurag Gupta ³, Mandeep Dhanda ¹, R. S. Walia ¹, Manoj Kumar ⁴, Ankit D. Oza ⁵, Dumitru Doru Burduhos-Nergis ^{6,*} and Diana Petronela Burduhos-Nergis ^{6,*}

¹ Department of Production & Industrial Engineering, Punjab Engineering College, Chandigarh 160012, India

² Central Scientific Instruments Organization (C.S.I.O.), Optical Devices and Systems Research Area (C.S.I.O.), Sector 30, Chandigarh 160030, India

³ Department of Mechanical Engineering, KIET Group of Institutions, Ghaziabad 201206, India

⁴ Department of Mechanical Engineering, Chandigarh University, Mohali 140413, India

⁵ Department of Computer Sciences and Engineering, Institute of Advanced Research, Gandhinagar 382426, India

⁶ Faculty of Materials Science and Engineering, Gheorghe Asachi Technical University of Iasi, 700050 Iasi, Romania

* Correspondence: doru.burduhos@tuiasi.ro (D.D.B.-N.); diana.burduhos@tuiasi.ro (D.P.B.-N.)



Citation: Vaishya, R.O.; Sharma, V.; Mishra, V.; Gupta, A.; Dhanda, M.; Walia, R.S.; Kumar, M.; Oza, A.D.; Burduhos-Nergis, D.D.; Burduhos-Nergis, D.P. Mathematical Modeling and Experimental Validation of Surface Roughness in Ball Burnishing Process. *Coatings* **2022**, *12*, 1506. <https://doi.org/10.3390/coatings12101506>

Academic Editor: Alexander Tolstoguzov

Received: 13 September 2022

Accepted: 6 October 2022

Published: 9 October 2022

Publisher's Note: MDPI stays neutral with regard to jurisdictional claims in published maps and institutional affiliations.



Copyright: © 2022 by the authors. Licensee MDPI, Basel, Switzerland. This article is an open access article distributed under the terms and conditions of the Creative Commons Attribution (CC BY) license (<https://creativecommons.org/licenses/by/4.0/>).

Abstract: Burnishing is a cold working technique used as a surface enrichment to meet the desired surface properties of the workpiece. It improves the visual properties, dimensional tolerances, fatigue strength, surface roughness, and hardness of the work material by applying appropriate pressure through a complex ball burnishing tool to cause plastic deformation. In the current work, the mathematical modeling of the burnishing process was carried out to predict surface roughness by considering the process parameters such as contact radius, penetration depth, and elastic rebound. Further, a customized tungsten carbide (W.C.) insert having a hardness of 80 HRC was developed for the burnishing operation. The micro-hardness of the resulting burnished surface improved from 44 to 48 HRC. The surface quality of the tungsten carbide insert improved by up to 17.1 nm through polishing. Several experiments were performed by selecting appropriate process parameters using developed model feedback. The surface quality of the workpiece improved by up to 45 nm, which resulted in automatic improvements in fatigue strength up to seven times that of the virgin material. The results predicted from the mathematical model were in good agreement (less than 5% deviation) with the experimental results. This study helps to understand the surface formation mechanism in the burnishing process in more detail. Additionally, the achieved results show a significant improvement in the surface finish (~95%), indicating the potential of the burnishing process and how fast and cost-effective it is. The novelty of this paper lies in the improvement in surface roughness and the validation of our mathematical model results with the experimental results.

Keywords: burnishing process; surface roughness; mathematical modeling; tungsten carbide; hardness

1. Introduction

In the recent decade, the finishing operation has been considered the most crucial criterion due to the development of advanced technology, new materials, and the work within various research areas in various fields. The different fields include aerospace, medical, and optical devices, as well as the automobile industry, which requires higher reliability, high performance, strength-to-weight ratio, and surface roughness. The finishing operations, such as diamond turning, may be replaced with the burnishing process as a similar surface finish can be achieved. However, due to its costlier nature, burnishing is still preferred in several cases. Nonconventional techniques for super-finishing require

honing and lapping, while conventional processes require milling, and the lathe operation generates a lot of chips. However, burnishing is a chip-less process where no metal removal takes place. As a result, cold working is effectively completed at a higher force. The higher force applied (by using pressure through a tungsten carbide insert with a radius of 6 mm) to a surface is more than the yield strength of the material, which results in plastic deformation; as a result, it enhances fatigue strength and hardness, and increases wear resistance.

Many researchers worldwide have worked on the burnishing process by conducting experimental and modeling techniques. A few of them are reported as the Taguchi method [1], and fuzzy logic [2] used to manipulate the input parameters of the burnishing process. Loh et al. [3] conducted experiments on AISI 1045 as the workpiece material, and considered ball material, depth of penetration, and force as input parameters. The TiC ball gave a better surface roughness than a steel ball-bearing. Morimoto et al. [4] worked on five different materials: SiC, alumina, ceramic, bearing steel, and cemented carbide, and found that the cemented carbide ball gave better results. Klocke and Liermann [5] considered ceramic as a ball material and found a 40% reduction in valleys and compressive stresses developed on the surface. Shiou and Chen [6] worked on plastic injection mold steel PDS5 and considered a tungsten carbide ball and speed, feed, and burnishing force as process parameters. Yeldose and Ramamoorthy [7] worked on steel, with input parameters of speed, feed, number of passes, and burnishing force, and considered TiN-coated and uncoated rollers, finding that a TiN-coating improved surface roughness. The main plus points of experimental methods were high pertinence, easily conductible, and well recognized worldwide. Still, the implications of experimental methods are wrong, meaning experimental data applied in experiments cannot be applied to other investigations.

In the recent decade, the development of technology modeling based on finite element analysis (FEA) has caught the eyes of a new generation of scholars, and many researchers have made valuable contributions. Skalski et al. [8] developed a model for the burnishing process, considering elastic-plastic properties and stick-slip friction for the analysis of contact deformations. Mustafa Kuntoğlu et al. [9] studied flank wear, surface roughness, cutting force, acoustic emissions, and chips morphology were considered under dry turning conditions for the comparison of the effect of cutting speed, feed rate and cutting tool hardness. Mustafa Kuntoğlu et al. [10] investigated the optimization of five different sensorial criteria, in addition to tool wear (V_B) and surface roughness (R_a), via the Tool Condition Monitoring System (TCMS) for the first time in the open literature. Based on the Taguchi L9 orthogonal design principle, the basic machining parameters cutting speed (v_c), feed rate (f), and depth of cut (a_p) were adopted for the turning of AISI 5140 steel. Bouzid and Sa [11] worked on AISI-1042 steel and conducted an FEA. analysis to find the displacement of material that considered the effect of elastic rebound of material, and calculated compressive stress. Mustafa Kuntoğlu et al. [12] used indirect tool condition and monitoring systems to provide tracking for the condition of the cutting tool via several released or converted energy types, namely, heat, acoustic emission, vibration, cutting forces and motor current. Yen et al. [13] regarded hard rollers as roller material and conducted two-dimensional and three-dimensional analyses for compressive stress and material displacement. Uddin and Hall [14] worked on AZ31B Magnesium alloy, considered a 10 mm steel ball as the ball material for deep ball burnishing, and conducted a three-dimensional FEA analysis. In the study of A. A. Ibrahim [15], the literature revealed that when the surface finish improved by around 70%, the fatigue strength improved seven times that of the virgin material. However, fatigue life, which is measured in terms of the number of cycles, improved after the burnishing procedure. In general, burnished specimens are reported to have a substantially longer fatigue life than the original sample. Beres and Patnaik [16] conducted a two-dimensional and three-dimensional study of the burnishing process and found compressive stress distribution and plane plastic strains. Sartkulvanich and Altan [16] considered the ceramic ball a ball material and conducted two-dimensional and three-dimensional analyses to predict surface roughness and compressive stresses.

Zhuang and wicks [17] worked on aircraft engine components and conducted a three-dimensional study of the complex pressure generated due to cyclic plastic deformation. Salahshoor and Guo [18] worked on a Ti6Al4V workpiece that considered the ceramic ball as a ball material and developed a three-dimensional analysis for compressive stresses and surface roughness. Mounira Bourebiaa in [19] mentions that burnishing imparts a superficial hardness improvement to the surface. This increase in surface hardness caused by burnishing is caused by the plastic deformation of new superficial layers that are hardened with a fine texture and elongated. In this study, mathematical modeling for predicting the surface roughness of a workpiece after burnishing with a tungsten carbide insert was derived, and the relationship between surface roughness and input parameters, including burnishing force, workpiece diameter, and insert diameter, was established. Experiments were carried out on a Stavax workpiece with a diameter of 60 mm and a hardness of 44 HRC for measuring surface roughness, and results were obtained from the mathematical model and experimentally verified. In this paper, mathematical modeling of the burnishing process has been presented to predict surface roughness. Further, the customized tungsten carbide (W.C.) insert is developed, impacting/improving its surface quality. The different finite element method (FEM) models have been developed, along with residual stress [20–22].

Figure 1 shows the flow chart of the burnishing process. It starts from its mechanism with the insert preparation, modeling, experimentation, results and validation. These modules further subdivide, as indicated in Figure 1. After machining the workpiece consisting of peaks and valleys of different heights, the plastic deformation occurs by applying force beyond the yield strength using the ball burnishing as a tool. Owing to the applied force, the workpiece deforms peaks into valleys, improves surface finish results, increases fatigue strength and hardness, and increases wear resistance and corrosion. These effective properties attract many industries of small scale that do not get diamond turning to achieve almost the same level of finish achieved by the TiC-insert burnishing process, as shown in Figure 2.

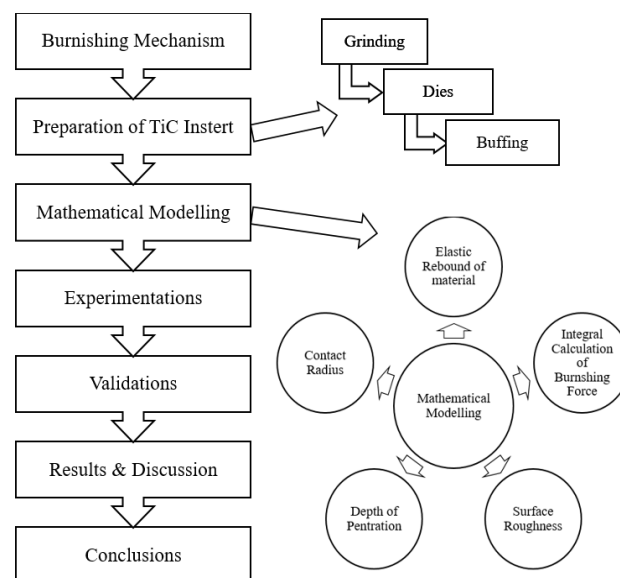


Figure 1. A flow chart of the burnishing process.

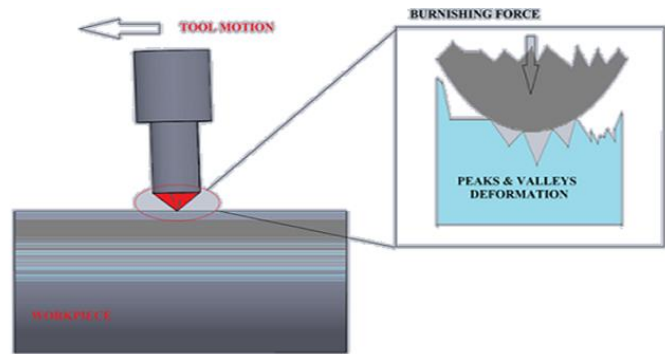


Figure 2. Burnishing mechanism.

2. Materials and Methods

The tungsten carbide material is selected as a burnishing tool material due to its high hardness, i.e., 80 HRC and thermal stability. The rod of 15 mm in length and diameter of 10 mm is used for tool development. The grinding process forms a radius of 6 mm on one side of the tool. Buffing and polishing are performed to improve the surface finish on the curved side. Diamond paste is used for precision polishing. All of the development for burnishing tools is completed with conventional grinding and polishing processes to make it cost-effective. The surface is characterized using a contact type profilometer from Taylor Hobson-made Talysurf PGI-120 (Bengaluru, India). The tool’s radius is 5.8 mm, with a surface finish of 17.1 nm. The results for tool radius, finish, and the basic tool insert is shown in Figure 3.

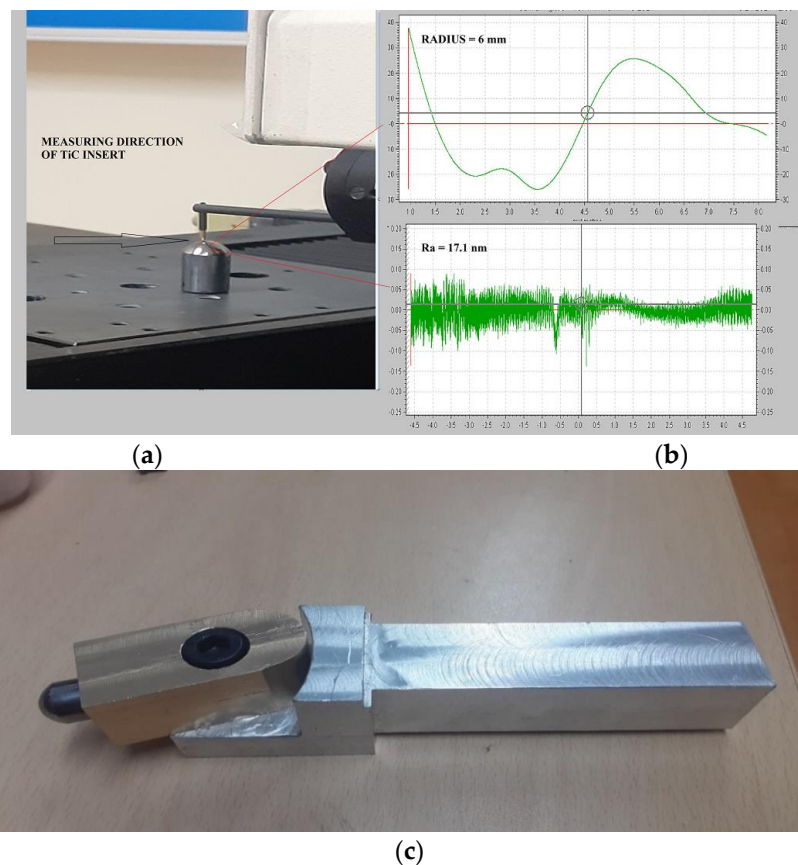


Figure 3. (a) Surface roughness measurement, (b) radius profile of insert, (c) actual tool insert.

3. Mathematical Modeling

3.1. Contact Radius (Z)

Assumptions based on Hertz Contact Theory [12]:

1. The two interacting bodies are assumed to be of an elastic, isotropic and homogenous material.
2. The strains are small and within the elastic limit.
3. The surfaces are continuous and nonconforming.
4. There is non-adhesive contact between surfaces.
5. The surface is assumed to be perfectly smooth such that no shear stresses occur in the interacting surfaces.
6. The Surface is frictionless.
7. Workpiece considered elastoplastic.
8. Each solid is considered an elastic half-space. i.e., the area of contact is much smaller than the characteristic radius of the body.
9. It is assumed that only a relatively small part of the total surfaces is in contact.

Figure 4 shows the cross-section to find the contact radius where symbol representation is as; r_1 —ball radius; r_2 —workpiece radius; E_1 —ball elastic modulus; E_2 —workpiece elastic modulus; ν_1 and ν_2 —Poisson ratios of ball and workpiece, respectively; F —burnishing force acting vertically; These equations find the radius (Z) of the contact radius; $2a$ and $2b$ —the major and minor axis of the ellipse, respectively.

$$\frac{x^2}{a^2} + \frac{y^2}{b^2} = 1 \quad (1)$$

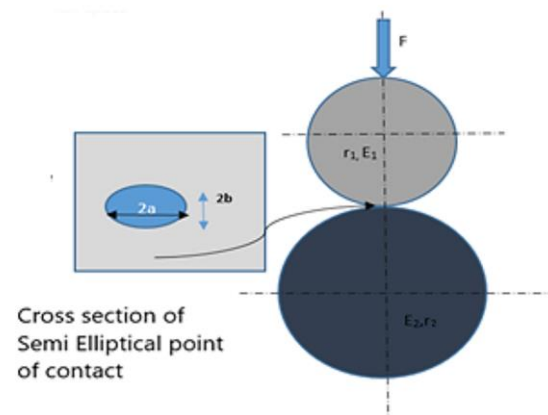


Figure 4. Cross-section to find contact radius.

Area of the ellipse

$$A = \pi ab \quad (2)$$

e is the eccentricity of the ellipse given by

$$e^2 = 1 - \frac{b^2}{a^2} \quad (3)$$

Now, the relation between the major and minor axis concerning the radius of the ball and workpiece

$$b^2 = 1 *^{4/3} (r_2) \quad (4)$$

$$a^2 = 1 *^{4/3} (r_1) \quad (5)$$

The relative radius is given by

$$R_c = (r_1 * r_2)^{\frac{1}{2}} \tag{6}$$

Elastic Modulus (E) in terms of Poisson ratio is given by

$$\frac{1}{E^*} = 1 - \nu^2/E^1 + 1 - (\nu_2)^2/E^2 \tag{7}$$

Now radius (Z) of the contact radius is

$$Z = \sqrt{a.b} = \sqrt[3]{\frac{3R_c * F}{4E^*}} \tag{8}$$

by using Equations (3)–(6); Now, by substitution of value R_c and E^*

$$z = \sqrt[3]{(3F * \sqrt{r_1 r_2} * 1 - \nu^2/E^1 + 1 - (\nu_2)^2/E^2)^{\frac{1}{4}}} \tag{9}$$

3.2. Depth of Penetration

Figure 5 shows the ball indented in the workpiece and the penetration depth. Then, to find the depth of penetration, (Δ) is related to Maximum force along with the radius of contact, which is given as

$$\Delta = Z^2/R_c \tag{10}$$

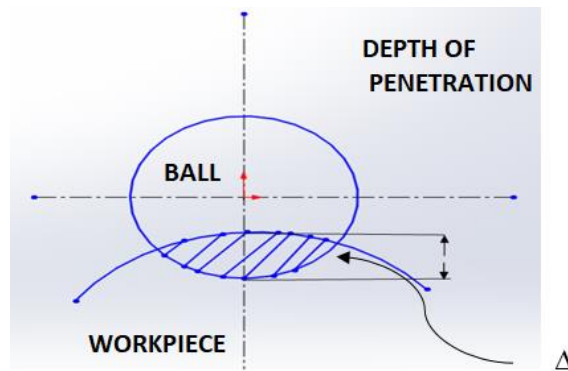


Figure 5. Depth of penetration.

Now by substitution of values in equation from Equations (6) and (9)

$$\Delta = \left(\sqrt[3]{(3F * \sqrt{r_1 r_2} * (1 - \nu^2/E^1 + 1 - (\nu_2)^2/E^2)^{\frac{1}{4}})} \right)^2 / (r_1 * r_2)^{\frac{1}{2}}$$

By solving this equation, we get

$$\Delta = \frac{9^{1/3}}{16^{1/3}} * F^{2/3} * (1 - \nu^2/E^1 + 1 - (\nu_2)^2/E^2)^{\frac{2}{3}} / (r_1 * r_2)^{\frac{1}{6}}$$

3.3. Integral Calculation of Burnishing Force $F(x, y)$

The elliptical zone is created when the burnishing process force is applied to the workpiece surface. The semi-minor axis of the oval zone that varies from $(-b < y < +b)$ comes into the picture to calculate the total burnishing force over a contact area. The cross-section view of deformation shown in Figure 6 should be integrated along the minor axis to calculate F . The depth of penetration Δ is directly dependent on the burnishing force $F(x, y)$.

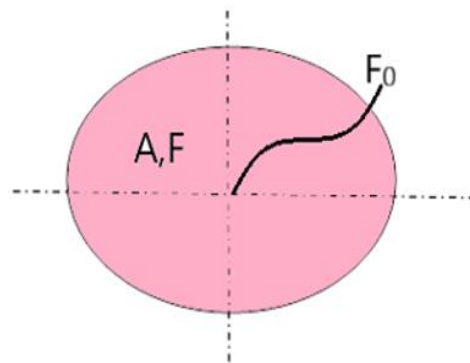


Figure 6. Integral force in the system.

A is an area of contact region in the form of an ellipse; $F(x, y)$ is the burnishing force over an entire region; F_0 is the burnishing force at a point O whose value is $3F/2 \times 3.14 \times a \times b$.

Now the concentrated load of the distribution function in the short minor axis over the contact area A is obtained using Equation (1)

$$\frac{x^2}{a^2} + \frac{y^2}{b^2} = 1$$

$$F(x, y) = F_0 \left(1 - \frac{x^2}{a^2} + \frac{y^2}{b^2}\right)^n \tag{11}$$

The power of n is obtained through contact between the ball and the workpiece. As an elliptical point of contact, the value of n is $1/2$.

Now force distribution over the contact area is represented as

$$F(x, y) = F_0 * \left(1 - \frac{x^2}{a^2} + \frac{y^2}{b^2}\right)^{1/2}$$

As force occurs in the minor axis, F_b is given as

$$F_b = 2 * \int_0^b F(x, y) dy \tag{12}$$

3.4. Integral Calculation of Burnishing Force $F(x, y)$

Plastic deformation occurs when the burnishing tool comes in contact with the peaks and valleys of the surface by applying force beyond the yield strength. Still, elastic deformation also occurs, but it is much smaller than plastic deformation, as shown in Figure 7. Therefore, the depth of penetration is not Δ ; it must be less than it.

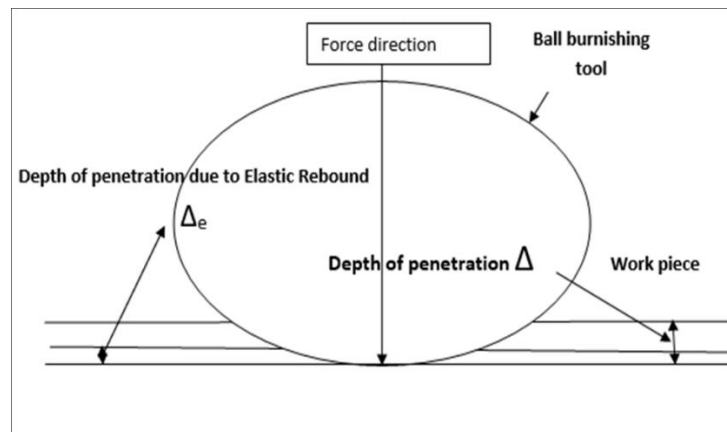


Figure 7. Elastic rebound of material.

For the calculation of the depth of penetration due to elastic rebound (Δ_e):
 As the applied force is beyond the yield strength, von Mises takes place for the elastoplastic material.

Therefore, some stress–strain is generated given by the equation

$$\alpha = \varphi\beta \quad \beta \leq \beta_s \tag{13}$$

$$\alpha = \alpha_s + \forall(\beta - \beta_s) \quad \beta \geq \beta_s \tag{14}$$

$$\beta_s = \frac{\sqrt{2}}{2} (\sqrt{(\sigma_1 - \sigma_2)^2 + (\sigma_2 - \sigma_3)^2 + (\sigma_3 - \sigma_1)^2})$$

α —stress; φ —Young’s Modulus; β —strain; α_s —stress during yield stress; \forall is strain hardening of material; β_s —material yield stress; $\sigma_1, \sigma_2, \sigma_3$ are the principal stresses in x, y, z direction that occur; shear stress = 0.

As there is a point contact between the tool and workpiece, and the concentrated force over region A, internal stresses generated in the elastic region, as given by Flamant [13] are

$$\begin{aligned} \sigma_1 &= -2 * F_b * \cos\varnothing * \frac{1}{\pi * \text{radius of work - piece}} \\ \sigma_2 &= 0 \\ \sigma_3 &= -2 * v_2 * F_b * \cos\varnothing * \frac{1}{\pi * \text{radius of work - piece}} \end{aligned}$$

3.5. Integral Calculation of Burnishing Force $F(x, y)$

Depth of penetration due to elastic rebound (Δ_e) is found as the integral of strain in the Z direction, and strain is calculated as stress in that direction/Young’s modulus of Workpiece

$$\begin{aligned} \Delta_e &= 2 \int_0^{t/10} \sigma_3 dz \\ \Delta_e &= \int_0^{t/10} -2 * v_2 * F_b * \cos\varnothing * \frac{1}{\pi * \text{radius of work - piece}} dz \end{aligned} \tag{15}$$

Therefore, surface roughness is calculated as

$$R_s = \Delta - \Delta_e$$

$$R_s = \frac{9^{1/3}}{16^{1/3}} * F^{2/3} * \left(\frac{1 - v^2}{E^1} + \frac{1 - (v_2)^2}{E^2} \right) \frac{2}{3} / (r_1 * r_2)^{1/6} - \frac{1}{5} * v_2 * F_b * \cos\varnothing * \frac{1}{\pi * \text{radius of work - piece}} * z^{1/10} \tag{16}$$

4. Results and Discussion

A tungsten carbide insert (burnishing tool) is held in the tool holder and the live center workpiece, as shown in Figure 8. During the burnishing experimentation, the force increases with the increases in depth of cut and the number of passes. The central part is a tungsten carbide insert of radius 6 mm, 15 mm in length, and 10 mm in diameter with a surface roughness of 17.1 nanometers and a hardness of 80 HRC.

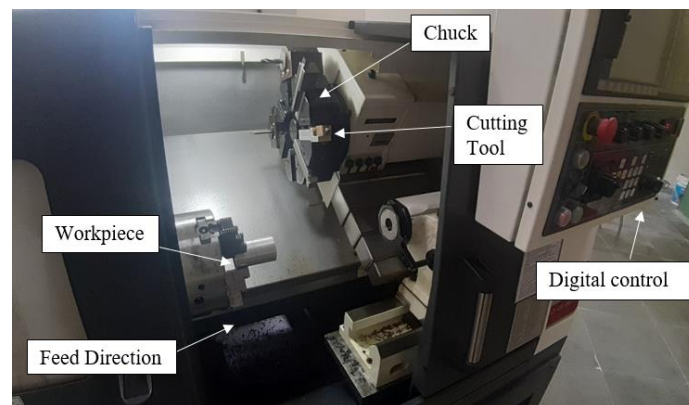


Figure 8. A complete view of SIEMENS CNC along with Tungsten Carbide Insert.

The workpiece material used for the experiment was Stavax. This material is often used in optical molds. The Stavax workpiece material was 60 mm in diameter and 100 mm in length, with a hardness of 44 HRC. The material composition was Carbon 0.38%, manganese 0.50%, chromium 13.60%, silicon 0.75%, and vanadium 0.30%. The properties of Stavax ESR steel include excellent corrosion resistance. Stavax ESR is a corrosion-resistant, through-hardening plastic mold steel with an excellent finish. The initial surface roughness of the workpiece is 5 microns. The machine used for measuring surface roughness was a Taylor Hobson CCI (Coherence Correlation Interferometer). The CCI is a noncontact 3D Optical Profiler with a thin and thick film measurement capability.

It uses an innovative, patented correlation algorithm to seek out the coherence peak and phase position of an interference pattern produced by the precision optical scanning unit, as shown in Figure 9.

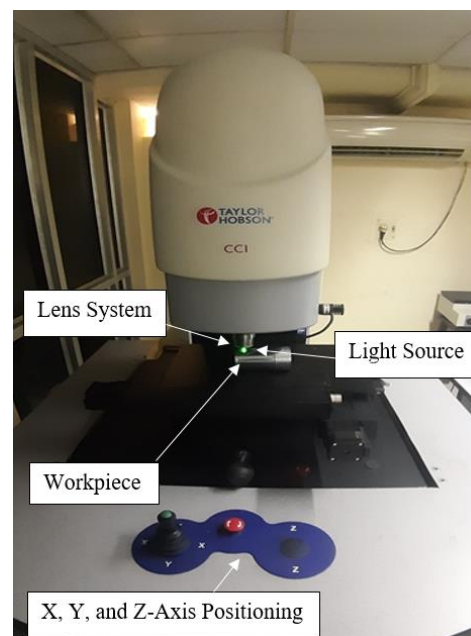


Figure 9. Workpiece placed under CCI for measuring surface roughness.

The workpiece of diameter 60 mm and length of 100 mm, with the help of tungsten carbide, with an insert burnishing tool feed rate of 10 microns, with four passes, at a speed of 400–600 rpm, and a depth of cut 0.02 micron as the input parameter and surface roughness as the considered output parameter. The experiments were performed under the given conditions and the surface roughness was measured with the help of the Taylor

Hobson CCI three-dimensional optical profiler. Figure 10 shows the final mirror-like surface finish on the Stavax workpiece.

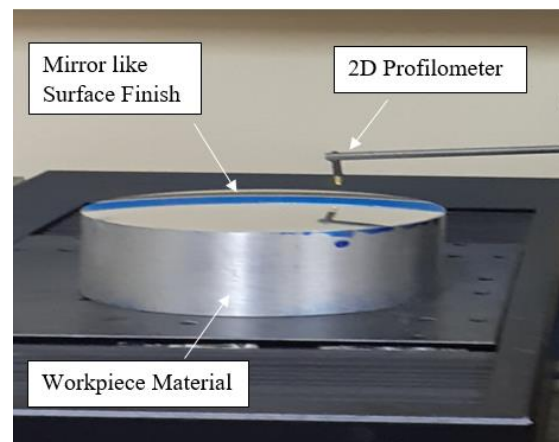


Figure 10. The final mirror-like surface finish on the Stavax workpiece.

Figures 11 and 12 describe the three-dimensional surface roughness profile and the two-dimensional surface profile initially and after burnishing under the defined conditions. Figure 11a–d describes the three-dimensional surface roughness, initial two-dimensional surface profile and after burnishing at a speed of 600 rpm with a depth of cut of 0.02 microns, a feed rate of 10 microns, and after four passes. Figure 11a describes the initial three-dimensional surface profile compared with the burnished surface profile in Figure 11b at 600 rpm, where the surface roughness improved from 5 microns to 87 nanometers. Figure 11c describes a two-dimensional profile compared with a burnished profile in Figure 11d at 600 rpm, where the surface roughness improved from 0.697 microns to 77 nanometers. There is an improvement of 95.65% and 88.95% in average surface roughness (S_a and R_a), respectively.

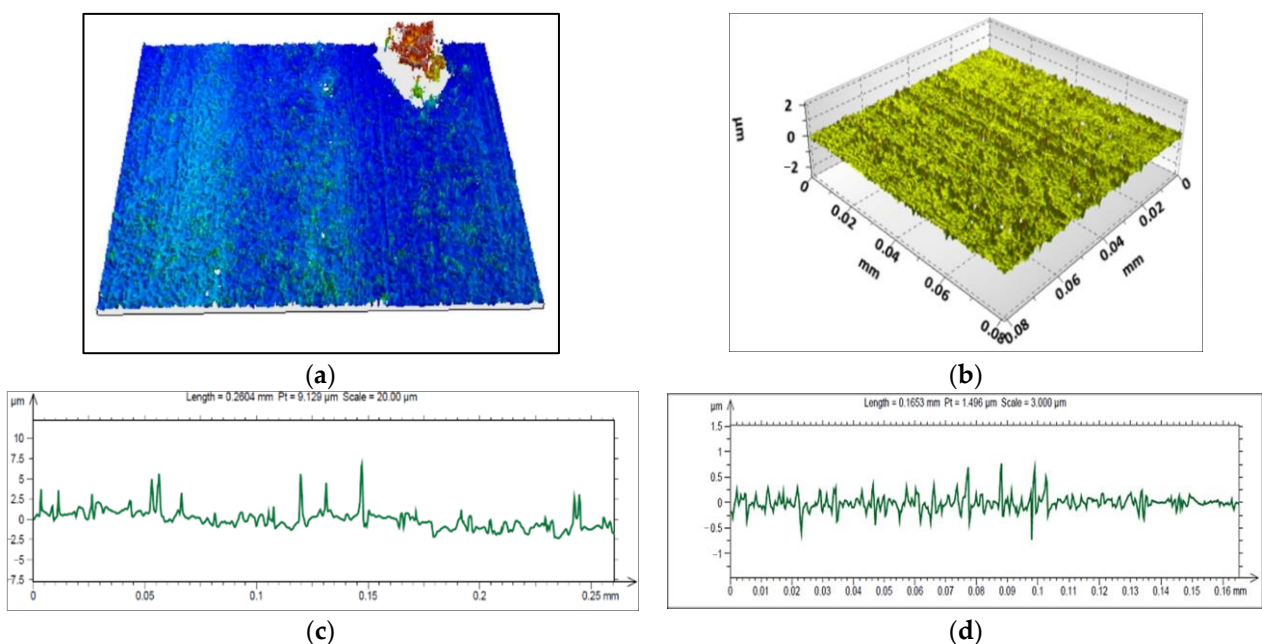


Figure 11. Differentiation of three–dimensional surface roughness, two–dimensional surface profile initially and after burnishing at 600 rpm. (a) 3D profile of initial surface, (b) 3D profile of burnished surface, (c) 2D profile of initial surface, (d) 2D profile of burnished surface.

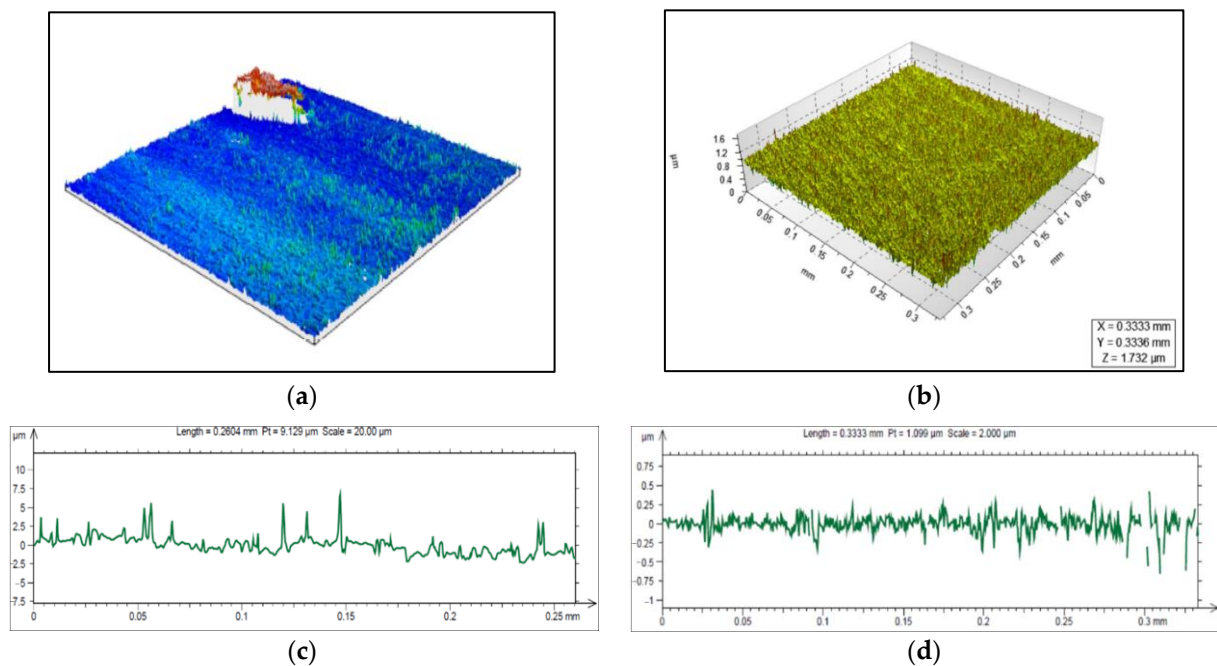


Figure 12. Differentiation of three-dimensional surface roughness, two-dimensional surface profile initially and after burnishing at 400 rpm: (a) 3D profile of initial surface, (b) 3D profile of burnished surface, (c) 2D profile of initial surface, (d) 2D profile of burnished surface.

Figure 12a describes the initial three-dimensional surface profile compared with the burnished surface profile in Figure 12b at 400 rpm, where the surface roughness improved from 5 microns to 60 nanometers. Figure 12c describes a two-dimensional shape compared with a burnished profile in Figure 12d at 400 rpm, where the surface roughness improved from 0.697 microns to 47 nanometers. There is an improvement of 97% and 93.25% in average surface roughness (Sa and Ra), respectively. Figure 12c describes the initial three-dimensional surface profile compared with the burnished surface profile in Figure 12d at 400 rpm, where the surface roughness improved from 5 microns to 60 nanometers. With each pass, the depth of cut was increased by 0.02 microns. Consequently, the burnishing force increased, resulting in peaks and valleys on the surface getting deformed and improving the surface roughness result, which is depicted by the three-dimensional surface profile of the burnished surface at 400 rpm.

Further, Figure 13 shows the close agreement of the developed model with actual experiments. Results predicted from the mathematical modeling of surface roughness are at 1% deviation from experimental results at 600 rpm, as shown in Figure 13a. The main essential thing from the results for both the mathematical modeling and experimentation methods is that they follow an almost identical trend. Surface roughness from the experimental approach is 87 nanometers, which is larger than the results from the predicted mathematical modeling of 77 nanometers because of the machining challenges of Stavax. Apart from that, certainty is assumed while deriving mathematical models such as non-adhesive contact between surfaces. The surface is frictionless, and the work-piece is considered elastoplastic, which is impossible while conducting experiments under these conditions.

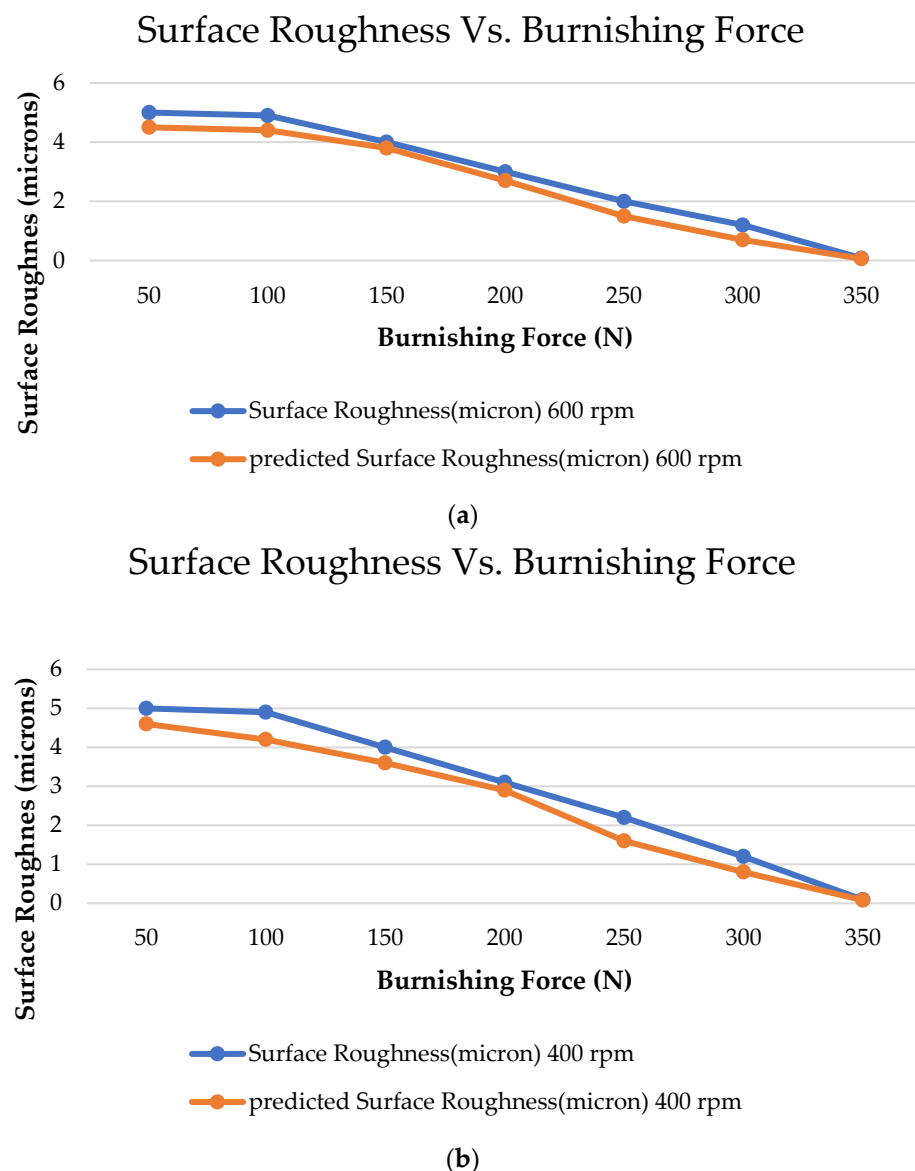


Figure 13. Comparison between experimental results and mathematical results. (a) surface roughness at 600 rpm, (b) surface roughness at 400 rpm.

Results predicted from the mathematical modeling of surface roughness and the experimental method at 400 rpm are at 1% deviation from experimental results, as shown in Figure 13b. The main essential result from mathematical modeling and experimentation is that they follow the same trend. Surface roughness from the experimental approach is 47 nanometers larger than the results from the predicted mathematical modeling of 35 nanometers.

Figure 11a describes the initial three-dimensional surface profile compared with the burnished surface profile in Figure 11b at 600 rpm, where the surface roughness improved from 5 microns to 87 nanometers. After each pass, the burnishing force increases; as a result, peaks and valleys on the surface get deformed, improving the surface roughness result, as depicted by the three-dimensional surface profile of the burnished surface at 600 rpm.

5. Conclusions

In this study, mathematical modeling was derived for predicting the surface roughness (R_a) of the workpiece using a tungsten carbide insert burnishing tool. The relationship between the surface roughness and input parameters was established (including burnishing

force, workpiece diameter, and insert diameter). Experiments were carried out to measure the surface roughness, and results were obtained. Results obtained from the mathematical model and experimental results were verified. The following conclusions may be drawn from the present study:

1. Experimental results using the TiC insert for the burnishing process reduced surface roughness (considering a 10 micron feed rate, 0.02 micron depth of cut, and 400–600 rpm).
2. There was a close agreement between the results obtained from mathematical modeling and the experimental results. A slight variation was observed, which might be due to the assumptions made during model development.
3. Burnishing imparts a superficial hardness to the surface. The micro-hardness of the resulting burnished surface improved from 44 to 48 HRC. This increase in surface hardness was due to the burnishing process, which causes the plastic deformation of new superficial layers that are hardened with a fine texture and elongated.
4. There is a significant improvement of 95.65% and 88.95% in average surface roughness (S_a and R_a), respectively, at 600 rpm. Similarly, a 97% and 93.25% improvement in average surface roughness (S_a and R_a), respectively, were also observed at 400 rpm.
5. A mirror-like surface finish was observed on the workpiece after employing the parametric combinations. However, the surface finish was mainly dependent upon the parametric combinations. Future research to measure surface roughness could be carried out by varying rpm and using different inserts.
6. The conducted tests revealed that when a sample is burnished, the force should not exceed 350 N, otherwise metal flakes will be formed. However, increasing the burnishing force increases the depth of the hardened layer. Surface hardness increases at these high forces until it reaches a limit beyond which flaking of the metal occurs. As a result of the lower efficiency and failure of the workpiece, a smaller burnishing force of 350 N was used. The 350 N sample did not result in the flaking of the subsurface layer.
7. It was also observed that the surface finish improved around 70%, and the fatigue strength improved seven times that of the virgin material; as in our experimentation, the surface roughness improved from 80% to 90% (from 400–600 rpm). Therefore, we can say that the fatigue strength of the components improved by 7 to 8% of the virgin material. However, fatigue life which is measured in terms of the number of cycles, improved after the burnishing procedure. In general, the burnished specimens were reported to have a substantially longer fatigue life than the original sample.

Author Contributions: R.O.V.—Conceptualization, writing—original draft preparation; V.S.—methodology, writing—original draft preparation; V.M.—formal analysis, data curation, methodology; A.G.—methodology, data curation; M.D.—project administration, formal analysis, data curation; R.S.W.—investigation, methodology; M.K.—validation, investigation; A.D.O.—writing—original draft preparation, formal analysis; D.D.B.-N.—writing—review and editing, funding acquisition; D.P.B.-N.—writing—review and editing, funding acquisition. All authors have read and agreed to the published version of the manuscript.

Funding: This work was supported by the Gheorghe Asachi Technical University of Iași—TUIASI-Romania, Scientific Research Funds, FCSU-2022.

Institutional Review Board Statement: Not applicable.

Informed Consent Statement: Not applicable.

Data Availability Statement: The authors confirm that the data supporting the findings of this study are available within the article.

Acknowledgments: This paper was realized with the support of “Institutional development through increasing the innovation, development and research performance of TUIASI—COMPETE”, project funded by contract no. 27PFE /2021, financed by the Romanian government. This paper was

also supported by “Gheorghe Asachi” Technical University from Iași (TUIASI), through the Project “Performance and excellence in postdoctoral research 2022”.

Conflicts of Interest: The authors declare no conflict of interest.

References

1. El-Taweel, T.A.; El-Axir, M.H. Analysis and optimization of the ball burnishing process through the Taguchi technique. *Int. J. Adv. Manuf. Technol.* **2009**, *41*, 301–310. [[CrossRef](#)]
2. Basak, H.; Goktas, H.H. Burnishing process on Al-alloy and optimization of surface roughness and surface hardness by fuzzy logic. *Mater. Des.* **2009**, *30*, 1275–1281. [[CrossRef](#)]
3. Tam, N.H.; Loh, S.C.; Miyazawa, S. Surface hardening by ball burnishing. *Tribol. Int.* **1990**, *23*, 413–417.
4. Morimoto, T.; Tamamura, K. Burnishing process using a rotating ball-tool—Effect of tool material on the burnishing process. *Wear* **1991**, *147*, 185–193. [[CrossRef](#)]
5. Klocke, F.; Liermann, J. Roller burnishing of hard turned surfaces. *Int. J. Mach. Tools Manuf.* **1998**, *38*, 419–423. [[CrossRef](#)]
6. Shiou, F.J.; Chen, C.H. Freeform surface finish of plastic injection mold by using ball-burnishing process. *J. Mater. Process. Technol.* **2003**, *140*, 248–254. [[CrossRef](#)]
7. Yeldose, B.C.; Ramamoorthy, B. An investigation into the high performance of TiN-coated rollers in burnishing process. *J. Mater. Process. Technol.* **2008**, *207*, 350–355. [[CrossRef](#)]
8. Skalski, K.; Morawski, A.; Przybylski, W. Analysis of contact elastic-plastic strains during the process of burnishing. *Int. J. Mech. Sci.* **1995**, *37*, 461–472. [[CrossRef](#)]
9. Kuntoğlu, M.; Gupta, M.K.; Aslan, A.; Salur, E.; Garcia-Collado, A. *Influence of Tool Hardness on Tool Wear, Surface Roughness and Acoustic Emissions during Turning of AISI 1050*; IOP Publishing Ltd.: Bristol, UK, 2022.
10. Kuntoğlu, M.; Abdullah, A.; Hacı, S.; Danil, Y.P.; Khaled, G.; Tadeusz, M. Optimization and Analysis of Surface Roughness, Flank Wear and 5 Different Sensorial Data via Tool Condition Monitoring System in Turning of AISI 5140. *Sensors* **2020**, *20*, 4377. [[CrossRef](#)] [[PubMed](#)]
11. Bouzid, W.; Sa, K. Finite element modeling of burnishing of AISI 1042 steel. *Int. J. Adv. Manuf. Technol.* **2005**, *25*, 460–465. [[CrossRef](#)]
12. Kuntoğlu, M.; Aslan, A.; Pimenov, D.Y.; Usca, Ü.A.; Salur, E.; Gupta, M.K.; Mikolajczyk, T.; Giasin, K.; Kapłonek, W.; Sharma, S. A review of indirect tool condition monitoring systems and decision-making methods in turning: Critical analysis and trends. *Sensors* **2020**, *21*, 108. [[CrossRef](#)] [[PubMed](#)]
13. Yen, Y.C.; Sartkulvanich, P.; Altan, T. Finite element modeling of roller burnishing process. *CIRP Ann.* **2005**, *54*, 237–240. [[CrossRef](#)]
14. Uddin, M.S.; Hall, C.; Hooper, R.; Charrault, E.; Murphy, P.; Santos, V. Finite element analysis of surface integrity in deep ball-burnishing of a biodegradable AZ31B Mg alloy. *Metals* **2018**, *8*, 136. [[CrossRef](#)]
15. Ibrahim, A.A. Fatigue Life Enhancement of Carbon Steel by Ball Burnishing Process. *Mansoura Eng. J.* **2008**, *33*, 1–9. [[CrossRef](#)]
16. Johnson, K.L. *Contact Mechanics*; Cambridge University Press: Cambridge, UK, 1985.
17. Timoshenko, S.; Goodier, J.N. *Theory of Elasticity*, 3rd ed.; McGraw-Hill: New York, NY, USA, 1970.
18. Bourebia, M.; Bouri, A.; Hamadache, H.; Achouri, S.; Laouar, L.; Gharbi, A.; Ghelloudj, O.; Bouhamla, K. Study of the effect burnishing superficial hardness and hardening of S355JR steel using experimental planning. *Energy Procedia* **2019**, *157*, 568–577. [[CrossRef](#)]
19. Beres, W.; Li, J.; Patnaik, P.C. Numerical simulation of the low plasticity burnishing process for fatigue property enhancement. In *Turbo Expo: Power for Land, Sea, and Air*; ASME: New York, NY, USA, 2004; Volume 41693, pp. 809–818. [[CrossRef](#)]
20. Sartkulvanich, P.; Altan, T.; Jasso, F.; Rodriguez, C. Finite element modeling of hard roller burnishing: An analysis on the effects of process parameters upon surface finish and residual stresses. *J. Manuf. Sci. Eng.* **2007**, *129*, 705–716. [[CrossRef](#)]
21. Zhuang, W.; Wicks, B. Multipass low-plasticity burnishing induced residual stresses: Three-dimensional elastic-plastic finite element modelling. *Proc. Inst. Mech. Eng. Part C J. Mech. Eng. Sci.* **2004**, *218*, 663–668. [[CrossRef](#)]
22. Salahshoor, M.; Guo, Y.B. Finite element modeling of burnishing and the effects of process parameters on surface integrity of orthopedic implants. In *ASME International Mechanical Engineering Congress and Exposition*; ASME: New York, NY, USA, 2011; Volume 54884, pp. 489–498. [[CrossRef](#)]